NASA/TM—2000-209907

Double-Plate Penetration Equations

K.B. Hayashida and J.H. Robinson
Marshall Space Flight Center, Marshall Space Flight Center, Alabama

February 2000

The NASA STI Program Office...in Profile

Since its founding, NASA has been dedicated to the advancement of aeronautics and space science. The NASA Scientific and Technical Information (STI) Program Office plays a key part in helping NASA maintain this important role.

The NASA STI Program Office is operated by Langley Research Center, the lead center for NASA's scientific and technical information. The NASA STI Program Office provides access to the NASA STI Database, the largest collection of aeronautical and space science STI in the world. The Program Office is also NASA's institutional mechanism for disseminating the results of its research and development activities. These results are published by NASA in the NASA STI Report Series, which includes the following report types:

- TECHNICAL PUBLICATION. Reports of completed research or a major significant phase of research that present the results of NASA programs and include extensive data or theoretical analysis. Includes compilations of significant scientific and technical data and information deemed to be of continuing reference value. NASA's counterpart of peer-reviewed formal professional papers but has less stringent limitations on manuscript length and extent of graphic presentations.

- TECHNICAL MEMORANDUM. Scientific and technical findings that are preliminary or of specialized interest, e.g., quick release reports, working papers, and bibliographies that contain minimal annotation. Does not contain extensive analysis.

- CONTRACTOR REPORT. Scientific and technical findings by NASA-sponsored contractors and grantees.

- CONFERENCE PUBLICATION. Collected papers from scientific and technical conferences, symposia, seminars, or other meetings sponsored or cosponsored by NASA.

- SPECIAL PUBLICATION. Scientific, technical, or historical information from NASA programs, projects, and mission, often concerned with subjects having substantial public interest.

- TECHNICAL TRANSLATION. English-language translations of foreign scientific and technical material pertinent to NASA's mission.

Specialized services that complement the STI Program Office's diverse offerings include creating custom thesauri, building customized databases, organizing and publishing research results...even providing videos.

For more information about the NASA STI Program Office, see the following:

- Access the NASA STI Program Home Page at ***http://www.sti.nasa.gov***

- E-mail your question via the Internet to help@sti.nasa.gov

- Fax your question to the NASA Access Help Desk at (301) 621–0134

- Telephone the NASA Access Help Desk at (301) 621–0390

- Write to:
  NASA Access Help Desk
  NASA Center for AeroSpace Information
  7121 Standard Drive
  Hanover, MD 21076–1320

NASA/TM—2000–209907

Double-Plate Penetration Equations

K.B. Hayashida and J.H. Robinson
Marshall Space Flight Center, Marshall Space Flight Center, Alabama

National Aeronautics and
Space Administration

Marshall Space Flight Center

February 2000

Acknowledgments

The authors would like to acknowledge the assistance of those individuals who aided in the preparation of this document. William James was instrumental in obtaining source data, J.D. DeMarcos edited and critiqued the text, Doris Bailey typed the manuscript, and the staffs of the NASA Headquarters Library and the Scientific and Technical Information Program provided assistance in locating bibliographic references.

TRADEMARKS

Available from:

NASA Center for AeroSpace Information
7121 Standard Drive
Hanover, MD 21076–1320
(301) 621–0390

National Technical Information Service
5285 Port Royal Road
Springfield, VA 22161
(703) 487–4650

TABLE OF CONTENTS

LIST OF FIGURES

LIST OF TABLES

TECHNICAL MEMORANDUM

DOUBLE-PLATE PENETRATION EQUATIONS

1. INTRODUCTION

The potential threat from meteoroid and orbital debris particles impacting on pressurized spacecraft prompted a study of penetration predictor equations. Since the 1960's, many equations have been developed to predict the penetration of spacecraft structures by meteoroid particles. The recent rapid growth in the orbital debris environment emphasizes the need for further development of ballistic limit equations, for both single- and double-plate structures.[1] Because both meteoroids and orbital debris particles travel at hypervelocities, similar shielding is appropriate for both. The penetration predictor equations developed for meteoroids apply as well to orbital debris particles. In 1991, Hayashida and Robinson discussed the accuracy and effectiveness of five single-plate penetration predictor equations.[2] This paper is a continuation of that study, comparing the seven commonly used double-plate penetration predictor equations for their accuracy and effectiveness in the development of shield designs to protect spacecraft from the hazards of meteoroids and orbital debris.

In 1947, Fred Whipple was the first to propose placing a thin metal plate outboard of the spacecraft wall to improve the protection capability of the spacecraft from meteoroid particle impacts.[3] Hence, this double-plate structure is called the "Whipple shield." In this study, the thin metal plate is called the "bumper" plate, and the second plate, often the spacecraft structure itself, is called the "rear-wall" plate.

Each double-plate penetration predictor equation included in this study was developed with a unique set of test parameters. Actual conditions under which a spacecraft is required to survive may or may not be within the parameter range for an equation. Therefore, extreme care must be taken when using any penetration predictor equation since each is valid only for a specific set of parameters. After some study of test parameters, it becomes obvious that the majority of expected projectile velocities cannot be tested with current particle launcher technology. Theoretical predictions must be relied upon for high-velocity occurrences until further advances can be made in hypervelocity impact testing technology.

It is not the purpose of this paper to recommend any specific equation to use in analyzing a spacecraft; rather, the paper is a brief synopsis of seven common penetration predictor equations and a comparison of them. This provides a designer a better understanding of how a structure withstands hypervelocity impacts of meteoroid or orbital debris particles. Hypervelocity impact tests should always be included in the design and verification schedules for any spacecraft component which will be exposed to the meteoroid and orbital debris environments for any length of time.

In addition to protecting the spacecraft, the designer should also consider the potentially hazardous effects a damaged spacecraft can impose on other spacecraft in nearby or crossing orbits. Should a spacecraft break up or become uncontrollable due to a hypervelocity particle impact, it may have damaging effects on other spacecraft. A NASA Management Instruction, issued in April 1993, requires all new NASA programs to conduct formal assessments on each new spacecraft to determine the potential of generating new debris.[4] New debris is generated either through a slow breaking apart of a spacecraft or through a catastrophic explosion due to either particle impact or heating of contained gases. This debris would not only add to the debris environment but threaten other orbiting vehicles' survivability. NASA also issued a Safety Standard to guide designers through this assessment process.[5] Each component of the spacecraft should be carefully evaluated for the potential for new debris generation. Each spacecraft should have an acceptable reliability to indicate that neither a functional failure nor a failure that would affect other spacecraft will occur. Additionally, a spacecraft carrying a crew should also have an acceptable reliability for astronaut safety.

2. DOUBLE-PLATE PENETRATION EQUATIONS

In the 1960's, many penetration predictor equations for single- and double-plate structures were developed to predict meteoroid impact damage on spacecraft structures for the Apollo and other space programs. These equations were applicable for the extremely high-velocity impacts expected from interplanetary meteoroid sources.

There are three phases during a hypervelocity projectile impact onto a double-plate structure. The three phases are ballistic, shatter, and melt/vaporization (see fig. 1). Each phase has distinct characteristic effects on the impacting projectile, the bumper plate, and the rear-wall plate.

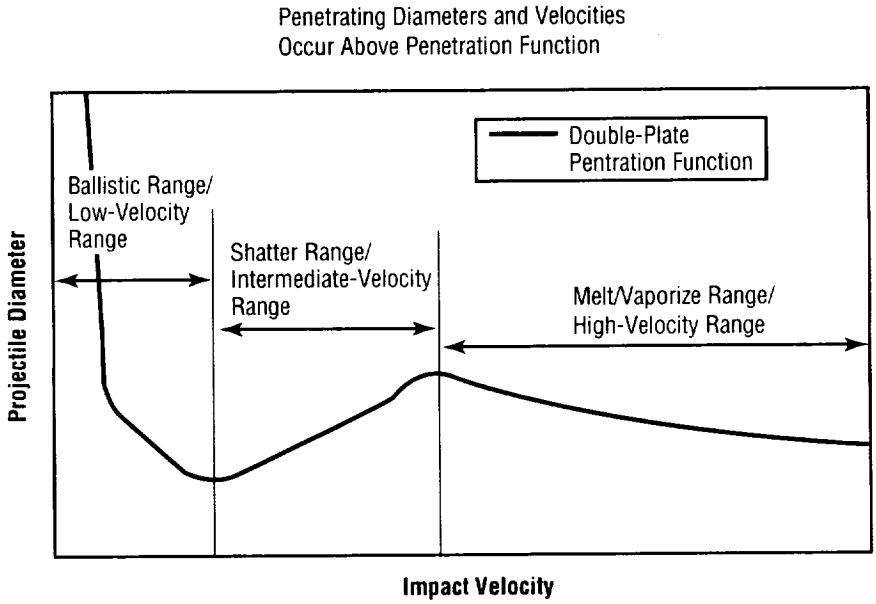

Figure 1. Three phase changes in double-plate penetration functions.

The ballistic phase occurs in the low-velocity range. The projectile travels too slowly to create a shock that could shatter the projectile upon impact. The intact projectile penetrates the bumper and impacts the rear-wall plate with a velocity and direction very similar to that of the initial particle. In the low-velocity range, double-plate structures react similarly to equivalent mass single-plate structures. The spacing between the plates has very little effect.

The shatter phase occurs in the intermediate-velocity range. The projectile impact creates a shock that begins to break the projectile apart at or around the impact point of the projectile. The shattered projectile material penetrates the bumper plate to create an expanding debris cloud of projectile and bumper plate materials. The expanding cloud dispurses the impact energy across an increasing area as it travels further away from the bumper plate. The small particles in the cloud impact the rear-wall plate

with less energy per area, and is thereby less damaging than in the ballistic phase. In the intermediate-velocity range the double-plate is a more effective structure than an equivalent single-plate. A double-plate structure can stop the debris cloud created by a much larger projectile. In this velocity range the spacing between the plates has a significant positive effect in stopping the debris cloud, due to its expansion over a larger area of the rear-wall plate as spacing is increased. However, after the spacing becomes large, the effect is no longer significant. This limit on spacing effectiveness must be determined by tests and analyses for each shield design.

The final phase is the melt/vaporization phase which occurs in the high-velocity range. The projectile and bumper plate material melt and vaporize upon projectile impact. As the projectile material penetrates the bumper plate, it creates a debris cloud of molten and vaporized projectile and bumper plate materials. As in the intermediate-velocity range, this combined debris dispurses across an increasing area as it travels further away from the bumper plate. These many molten particles impact with the rear-wall plate. The energy expended in melting and vaporization allows double-plate structures to stop even larger projectiles traveling in the high-velocity range than in the intermediate-velocity range. However, as the projectile impact velocity increases, the energy of the projectile eventually overcomes the positive effects of the melting and vaporization of the projectile. The debris cloud created behind the bumper plate exerts a pressure pulse on the rear-wall plate, eventually leading to a bulging and tearing failure of the plate. In the high-velocity range, the double-plate is a more effective structure than an equivalent single-plate. In this velocity range the spacing between the plates has a significant positive effect in stopping the debris cloud, due to its expansion over a larger area of the rear-wall plate as spacing is increased. However, as in the intermediate range, after the spacing becomes large the effect is no longer significant. This limit on spacing effectiveness must be determined by tests and analyses for each shield design, and will likely differ from the limit found from impacts occuring in the intermediate-velocity range.

In sections 2.1 through 2.7, the seven double-plate penetration predictor equations will be discussed for their effectiveness and accuracy: the Cour-Palais equation, the "modified" Cour-Palais equation, the "new" Cour-Palais equation, the Nysmith equation, the Lundeberg-Stern-Bristow equation, the Burch equation, and the Wilkinson equation. Each equation has its merits and best area of specific application, based on its development parameters. None of the predictor equation developers published quantitative correlations to the data used to develop the equations, but seemed to rely on graphical comparison of the equations to data to show their accuracy.

The NASA Johnson Space Center (JSC) developed the first three penetration predictor equations; i.e., the original, modified, and new Cour-Palais equations. The original Cour-Palais equation was developed by using the test data generated during the Apollo program. The original Cour-Palais equation evolved into the "modified" Cour-Palais equation as more test data became available. These two equations were developed to predict the penetration of the rear-wall plate due solely to meteoroid particle impacts, and only considered the melt/vaporization phase of the projectiles. The expected impact velocities of meteoroid particles on a spacecraft are between 10 and 70 km/sec in low-Earth orbit (LEO) where they are assumed to melt or vaporize upon impact with the bumper plate. Finally, the "new" Cour-Palais equation evolved from the modified Cour-Palais equation in order to cover all three phase changes, to include the effects of manmade orbital debris impacts at expected velocities between 2 and 15 km/sec in LEO.

The NASA Ames Research Center (ARC) developed the fourth equation, the Nysmith equation; and the NASA Lewis Research Center (LeRC) developed the fifth equation, the Lundeberg-Stern-Bristow equation. These two equations were developed independently from the JSC efforts in the 1960's. The Lundeberg-Stern-Bristow equation was developed for multiple-plate structures, thereby including double-plate structures, but was only developed for normal projectile impacts.

The sixth equation, the Burch equation, was developed for the U.S. Air Force, based upon the Lundeberg-Stern-Bristow equation to include penetration predictions of oblique impacts. The Burch equation was also a multiple-plate structures penetration predictor equation.

The seventh and last equation, the Wilkinson equation, was a further development of an equation developed by the NASA Langley Research Center (LaRC), the Madden equation, which used the equations of linear plate theory to predict penetration of a double-plate structure.

In summary, most of the seven double-plate penetration equations were developed in the 1960's to predict the damage expected on double-plate structures from meteoroid particle impacts. The modified and new Cour-Palais equations, however, evolved from the original penetration predictor equation to include the orbital debris particle impact parameters as more test data became available. With any of these equations, the designer can predict the smallest projectile size which will completely penetrate the rear-wall plate for a given impact angle and velocity, and double-plate structure design. Projectiles larger than this predicted size (at the same impact velocity and angle) are expected to completely penetrate the rear-wall plate; smaller ones are not expected to penetrate the rear-wall plate. The following subsections will discuss each of these penetration predictor equations in detail.

2.1 Original Cour-Palais Equation

Burton G. Cour-Palais developed what is known as the "original" Cour-Palais equation with test data generated during the Apollo program and extrapolating the test data to the meteoroid particle impact conditions.[6,7] This equation is also called the "nonoptimum" Cour-Palais equation, since the condition of the rear-wall plate is governed by the solid fragments in the projectile and the bumper debris. The "optimum" condition occurs when the shield and projectile impact parameters are such that the projectile and the bumper debris are either completely melted or vaporized. The tests were performed at the Manned Spacecraft Center (currently JSC) hypervelocity impact (HVI) test facility. Cour-Palais' test results contained velocities ranging from 0.5 to 8.5 km/sec, with various aluminum alloy targets and with glass and aluminum (Al) alloy projectiles.

$$t_w = 0.055\left(\rho_p \rho_b\right)^{\frac{1}{6}} m_p^{\frac{1}{3}} \frac{V_n}{S^{0.5}} \left(\frac{70}{\sigma}\right)^{0.5} \quad \text{valid for } \frac{t_b}{d} \geq 0.1 \ ,$$

where

d = projectile diameter (cm)
t_b = bumper thickness (cm)
t_w = rear-wall thickness (cm)
ρ_p = projectile density (gm/cm^3)

ρ_b = bumper density (gm/cm^3)
m_p = projectile mass (gm)
θ = impact angle measured from surface normal (deg)
V = projectile velocity (km/sec)
V_n = normal component of projectile velocity (km/sec) = $V\cos\theta$
S = spacing between bumper and rear-wall (cm)
σ = rear-wall yield stress (ksi).

Units for all the terms are metric, with one exception: the term for the rear-wall yield stress uses English units. It becomes unitless in the equation since a fixed value of 70 ksi is assigned as a typical value for the yield stress of aluminum alloys.

Based upon experimental evidence, Cour-Palais suggested that increasing the spacing between the bumper and rear-wall becomes ineffective after the spacing reaches a value of 25 to 30 times the particle size.

2.2 Modified Cour-Palais Equation

Cour-Palais later modified the "original" or "nonoptimum" Cour-Palais equation using additional HVI test results from JSC, Marshall Space Flight Center (MSFC), and other test facilities.[8,9] The test parameters included velocities ranging from 6.5 to 7.5 km/sec, aluminum alloy targets with densities varying from 2.7 to 2.8 gm/cm^3, nylon, glass, and aluminum projectiles with densities varying from 1.14 to 2.8 gm/cm^3, and projectile diameters ranging from 0.04 cm (0.016 in.) to 1.9 cm (0.748 in.). A function of the projectile diameter, $Cd^{0.5}$ (where $C = 0.16\ \mathrm{cm^2 - sec/gm^{2/3} - km}$), replaces a constant from the "original" equation, 0.055. In addition, different conditions are recommended to validate use of the two equations. The validation condition for the "original" equation is that the ratio of bumper thickness to projectile diameter; i.e., t_b/d, must be 0.1 or greater. However, the conditions for the modified equation are that the normal component of the projectile velocity must be 6.5 km/sec or greater, and the ratio of the spacing between the bumper and the rear-wall to the projectile diameter must be 15 or greater.

$$t_w = Cd^{0.5}\left(\rho_p\rho_b\right)^{\frac{1}{6}} m_p^{\frac{1}{3}} \frac{V_n}{S^{0.5}}\left(\frac{70}{\sigma}\right)^{0.5} \quad \text{valid for } V_n \geq 6.5\ \mathrm{km/sec} \text{ and } \frac{S}{d} \geq 15\ ,$$

where

C = coefficient = 0.16 cm^2–sec/gm$^{2/3}$ – km
d = projectile diameter (cm)
t_w = rear-wall thickness (cm)
ρ_p = projectile density (gm/cm^3)
ρ_b = bumper density (gm/cm^3)
m_p = projectile mass (gm)
θ = impact angle measured from surface normal (deg)

V = projectile velocity (km/sec)
V_n = normal component of projectile velocity (km/sec) = $V\cos\theta$
S = spacing between bumper and rear-wall (cm)
σ = rear-wall yield stress (ksi).

Just as for the "original" equation, units used for all the terms in the modified Cour-Palais equation are metric, with one exception. Again, the term for the rear-wall yield stress uses English units.

2.3 New Cour-Palais Equation

The following equation is the latest double-plate predictor equation published by JSC, and is called the "new" Cour-Palais equation. It is based on the "modified" Cour-Palais equation, and includes the results from additional aluminum alloy projectile and target HVI test results.[10,11] This equation is sometimes called the "Christiansen" equation since it was developed by Eric Christiansen at JSC:

$$d = \left[\left(t_w\left(\frac{\sigma}{40}\right)^{0.5} + t_b\right) \Big/ \left(0.6(\cos\theta)^{\frac{5}{3}} \rho_p^{0.5} V^{\frac{2}{3}}\right)\right]^{\frac{18}{19}} \quad \text{valid for } V_n \leq 3 \text{ km/sec}$$

$$d = \left\{\left[\left(t_w\left(\frac{\sigma}{40}\right)^{0.5} + t_b\right) \Big/ \left(1.248\rho_p^{0.5}\cos\theta\right)\right]^{\frac{18}{19}} (1.75 - (V\cos\theta)/4)\right\}$$

$$+\left\{\left[1.071 t_w^{\frac{2}{3}} \rho_p^{-\frac{1}{3}} \rho_b^{-\frac{1}{9}} S^{\frac{1}{3}}\left(\frac{\sigma}{70}\right)^{\frac{1}{3}}\right]((V\cos\theta)/4 - 0.75)\right\}$$

$$\text{valid for } 3 \text{ km/sec} < V_n < 7 \text{ km/sec}$$

$$d = 3.918\, t_w^{\frac{2}{3}} \rho_p^{-\frac{1}{3}} \rho_b^{-\frac{1}{9}} (V\cos\theta)^{-\frac{2}{3}} S^{\frac{1}{3}}\left(\frac{\sigma}{70}\right)^{\frac{1}{3}} \quad \text{valid for } V_n \geq 7 \text{ km/sec} \ ,$$

where

d = projectile diameter (cm)
t_b = bumper thickness (cm)
t_w = rear-wall thickness (cm)
ρ_p = projectile density (gm/cm^3)

ρ_b = bumper density (gm/cm^3)
θ = impact angle measured from surface normal (deg)
V = projectile velocity (km/sec)
V_n = normal component of projectile velocity (km/sec) = $V\cos\theta$
S = spacing between bumper and rear-wall (cm)
σ = rear-wall yield stress (ksi).

The new Cour-Palais equation is the only equation in this paper which covers all three phase changes; i.e., ballistic, shatter, and melt/vaporization, of both meteoroid and orbital debris particle impacts. The equation can be applied to the low-end orbital debris impact velocities of 2 km/sec, all the way up to the higher 72 km/sec meteoroid impact velocities. The equations assume the ballistic phase occurs at or below 3 km/sec; the shatter phase between 3 and 7 km/sec; and the melt/vaporization phase at or above 7 km/sec. The new Cour-Palais equation is also the only equation formulated to directly determine the ballistic limit projectile size; all other equations are formulated to directly calculate minimum wall thickness or number of walls required to stop a given set of impacting particle parameters. This makes the new Cour-Palais equation an analysis-oriented equation rather than a design-oriented equation, a very convenient format since most M/OD work is analysis based.

2.4 Nysmith Equation

C. Robert Nysmith developed the following equation in 1969 with test data from the Hypervelocity Ballistic Range test facility at ARC.[12,13] Nysmith and Cour-Palais developed their penetration predictor equations independently. However, both equations were developed to predict the effects of a meteoroid particle impacting a double-plate structure. Nysmith's tests contained Pyrex® glass spherical projectiles with a density of 2.23 gm/cm^3 to simulate the brittle meteoroid particles. The projectile size of 3.18 mm (0.125 in.) in diameter was fixed in the test series, while the target parameters were varied to gain sufficient impact data to develop the equation. Other test parameters in this series of tests included velocities up to 8.8 km/sec (29,000 ft/sec); 2024–T3 aluminum alloy for both the bumper and rear-wall; bumper thicknesses between 0.81 mm (0.032 in.) and 1.24 mm (0.049 in.); rear-wall thicknesses between 1.63 mm (0.064 in.) and 3.18 mm (0.125 in.); and spacing (between the bumper and rear-wall) between 17.5 mm (0.69 in.) and 42.9 mm (1.69 in.). Only data from projectile impacts normal to the target were used to develop the equation.

$$\frac{t_w}{d} = \frac{5.08V^{0.278}}{\left(\frac{t_b}{d}\right)^{0.528}\left(\frac{S}{d}\right)^{1.39}} \text{ valid for } \frac{t_b}{d} < 0.5 \text{ and } \frac{t_w}{d} < 1 \quad ,$$

where

d = projectile diameter (mm)
t_b = bumper thickness (mm)
t_w = rear-wall thickness (mm)
S = spacing between bumper and rear-wall (mm)
V = projectile velocity (km/sec).

The parameters for the Nysmith equation do not include any material properties for the bumper or rear-wall, unlike other double-plate penetration equations, since only one aluminum alloy was used. The equation was not recommended for use outside the material test parameters used to develop it. However, it was recommended for use in the high-velocity range; i.e., 6 km/sec (20,000 ft/sec) and greater, expected meteoroid velocities. Nysmith observed that impact results obtained in the low-velocity range, <6 km/sec, were very different (more shattering and less vaporization) and therefore not applicable to the high-velocity range.[12]

2.5 Lundeberg-Stern-Bristow Equation

In 1965, J.F. Lundeberg, P.H. Stern, and R.J. Bristow developed the following equation for NASA LeRC with test data from the hypervelocity laboratories at the Boeing Company in Seattle, WA.[14] The Lundeberg-Stern-Bristow equation, like many other equations developed in the 1960's, was developed to predict the damage due to meteoroid particle impacts. The equation applies to multiple-plate structures, which includes double-plate structures. The Lundeberg-Stern-Bristow equation was developed for aluminum projectiles impacting aluminum targets, although 14 bumper materials and 8 low-density filler materials were tested. The bumper materials used were magnesium-lithium, magnesium, aluminum, 6Al–4V titanium, zinc, 301 and 321 stainless steel, 1095 steel, beryllium-copper, copper, TZM molybdenum, niobium, lead, tantalum, and tungsten. The filler materials used were polyurethane, polystyrene, Q-felt, "Dexiglas," glass, wool, and cork. The projectile materials used were aluminum, Pyrex, nickel, and "sapphire" (3.9 gm/cm^3). Most of the projectiles were spherical and ranged from 0.08 cm (0.031 in.) to 0.64 cm (0.250 in.) in diameter. Projectile impact velocities varied from 1.5 km/sec (5,000 ft/sec) to 8.2 km/sec (27,000 ft/sec). The plate thicknesses used in this test series ranged from 0.005 cm (0.002 in.) to 0.318 cm (0.125 in.), with up to 44 plates. Overall spacing of the plates was as high as 32.77 cm (12.9 in.). Many tests did not include filler materials between the plates.

$$N = F_1\left(\frac{V}{C}\right)^{-\frac{4}{3}}\left(\frac{t_2}{d}\right)^{-\frac{7}{12}}\left(\frac{S_1}{d}\right)^{-\frac{5}{12}} \quad \text{valid for } 0.7 < \frac{V}{C} < 2$$

and

$$F_1 = 2.42\left(\frac{t_1}{d}\right)^{-\frac{1}{3}} + 4.26\left(\frac{t_1}{d}\right)^{\frac{1}{3}} - 4.18 \ ,$$

where

N = number of sheets penetrated following the first sheet
d = projectile diameter (in.)
t_1 = thickness of first sheet (in.)
t_2 = thickness of second and each succeeding sheet (in.)
S_1 = spacing between first and second sheets (in.)
V = projectile velocity (ft/sec)
C = speed of sound in first sheet (ft/sec).

When "N" in the Lundeberg-Stern-Bristow equation is set to 1, the equation can be solved for the projectile size which will penetrate the rear-wall plate of a double-plate structure.

2.6 Burch Equation

G.T. Burch studied the characteristics of impact damage to multiple-plate structures to enable vehicle and weapon designers to provide sufficient protection from hypervelocity projectiles.[15] Burch identified ≈600 data points from a literature search, and compared them with the Lundeberg-Stern-Bristow multiple-plate penetration equation to determine its effectiveness and accuracy. Impact velocities used in these tests ranged from 3 km/sec (10,000 ft/sec) to 7.6 km/sec (25,000 ft/sec). The test parameters included aluminum and steel, used as both targets and projectiles, and two projectile shapes; i.e., spheres and short rods.

The Lundeberg-Stern-Bristow data and many of the other data from the literature search Burch performed were for normal impacts only. To predict penetration by oblique impacts, some double-plate penetration predictors use the normal component of the projectile velocity. During the course of his study, Burch developed penetration equations for flight-path (oblique) as well as normal-path penetration for aluminum projectiles impacting aluminum targets. To provide the missing oblique impact data, he conducted additional HVI tests for impact angles ranging from 0 to 60 deg off the target normal. The 2024–T3 aluminum target thicknesses ranged from 0.025 cm (0.010 in.) to 0.406 cm (0.160 in.), with overall spacings between ≈2.54 cm (1 in.) and 25.4 cm (10 in.). The 2017 aluminum projectiles were spheres ranging from 0.318 cm (0.125 in.) to 0.635 cm (0.25 in.) in diameter.

$$\text{Flight path penetration: } N_F = \left(F_1 + 0.63F_2\right)\left(\frac{V}{C}\right)^{-\frac{4}{3}}\left(\frac{t_2}{d}\right)^{-\frac{7}{12}}\left(\frac{S_1}{d}\right)^{-\frac{5}{12}}$$

$$\text{Normal path penetration: } N_N = F_3\left(\frac{d}{t_2}\right)\left(\frac{V}{C}\right)^{-\frac{4}{3}},$$

where

$$F_1 = 2.42\left(\frac{t_1}{d}\right)^{-\frac{1}{3}} + 4.26\left(\frac{t_1}{d}\right)^{\frac{1}{3}} - 4.18$$

$$F_2 = 0.5 - 1.87\left(\frac{t_1}{d}\right) + \left(5\frac{t_1}{d} - 1.6\right)\chi^3 + \left(1.7 - 12\frac{t_1}{d}\right)\chi \quad \text{valid for } \frac{t_1}{d} \le 0.32$$

$$\chi = \tan\theta - 0.5 \quad \text{valid for } 0 \text{ deg} < \theta \le 60 \text{ deg}$$

$$F_3 = 0.32\left(\frac{t_1}{d}\right)^{\frac{5}{6}} + 0.48\left(\frac{t_1}{d}\right)^{\frac{1}{3}}\sin^3\theta,$$

and where

N_F = number of sheets penetrated by flight-path component of debris following the first sheet

N_N = number of sheets penetrated by normal component of debris following the first sheet

V = projectile velocity (ft/sec)

d = projectile diameter (in.)

t_1 = thickness of first sheet (in.)

t_2 = thickness of second and each succeeding sheet (in.)

S_1 = spacing between first and second sheets (in.)

C = speed of sound in first sheet (ft/sec)

θ = impact angle (deg).

2.7 Wilkinson Equation

In 1967, Richard Madden developed a penetration predictor equation using the equations of linear plate theory to predict the ballistic limit of double-plate structures.[16] In 1969, J.P.D. Wilkinson further developed Madden's equation into what is now known as the Wilkinson equation.[17] The Wilkinson equation is based on two basic assumptions; the first is that the bumper completely fragments or vaporizes the incoming projectile, and the second is that the failure of the rear-wall occurs as a bulge and a final tearing, or petalling, of the material. The first assumption implies that the Wilkinson equation is valid for impact velocities >8 km/sec, for aluminum on aluminum impacts, since the incoming projectile is completely fragmented or vaporized. The second assumption implies that there is no spallation from the back of the rear-wall plate, since it is assumed to react as a perfectly elastic, plastic plate. Wilkinson used a hydrodynamic computer code to model the response of the rear-wall to help develop the equation, then he graphically compared his equation with existing test data covering several materials including aluminum, steel, cadmium, titanium, and others as the projectiles and targets to qualitatively show the effectiveness of the equation.

$$m_p = \frac{1.44 L_2 M_2 S^2}{V_n} \qquad \text{valid for } \frac{M_1}{\rho_p d} > 1$$

$$m_p = \left[\frac{1.44 \left(\frac{\pi}{6} \right)^{\frac{1}{3}} L_2 M_1 M_2 S^2}{\left(\rho_p \right)^{\frac{2}{3}} V_n} \right]^{\frac{3}{4}} \qquad \text{valid for } \frac{M_1}{\rho_p d} < 1$$

and

$$d = \left[\frac{6 m_p}{\pi \rho_p} \right]^{\frac{1}{3}},$$

where

d = projectile diameter (cm)
m_p = projectile mass (gm)
M_1 = mass per unit area for bumper (gm/cm^2)
M_2 = mass per unit area for rear-wall (gm/cm^2)
ρ_p = projectile density (gm/cm^3)
V = projectile velocity (km/sec)
V_n = normal component of projectile velocity (km/sec) = $V\cos\theta$
L_2 = rear-wall material constant (0.401 for 2219 aluminum)
S = spacing between bumper and rear-wall (cm)
θ = projectile impact angle off the target normal (deg).

After rearranging the Wilkinson equation to solve for the ballistic limit rear-wall thickness instead of ballistic limit projectile mass, the equation becomes:

$$t_w = \frac{0.364 d^4 \rho_p^2 V_n}{L_2 S^2 \rho_b t_b \rho_w} \quad \text{valid for } \frac{d\rho_p}{\rho_b t_b} > 1$$

$$t_w = \frac{0.364 d^3 \rho_p V_n}{L_2 S^2 \rho_w} \quad \text{valid for } \frac{d\rho_p}{\rho_b t_b} < 1 \quad ,$$

where

t_b = bumper thickness (cm)
t_w = rear-wall thickenss (cm)
ρ_b = bumper density (gm/cm^3)
ρ_w = rear-wall density (gm/cm^3).

Like many others, Wilkinson assumed vaporization of the projectiles when he developed the equation and did not consider the loading rate effects in the rear-wall, such as a spall. In the late 1980's, due to test and analysis results from the early NASA Space Station program, Norman Elfer suggested a modification to the Wilkinson equation.[18,19] This modification would account for a lower dispersion angle of the debris cloud behind the bumper caused by melting instead of complete vaporization of the projectile, Wilkinson's assumption. Then, in the early 1990's, Abbott and Bjorkman also suggested a revision due to momentum multiplication seen from test and hydrocode data for the collision of the projectile and bumper debris with the rear-wall plate.[20] They suggested using 80 percent of the projectile diameter predicted by the Wilkinson equation as an approximation of a more realistic but conservative ballistic limit projectile diameter. The equation with this change is generally referred to as the "modified" Wilkinson equation.

3. COMPARISONS OF EQUATIONS AND TEST RESULTS

It is often beneficial during design and analysis of M/OD shield systems to compare the results from various predictor equations. In the following sections, double-plate equations are compared to single-plate equations (sec. 3.1), to each other (sec. 3.2), and to test results (sec. 3.3). Some design considerations are also noted, to help the designer determine whether the single-plate or double-plate design is the better choice (sec. 3.4). The predictor equations comparisons are made to show relative differences of the predicted results. Each equation should be carefully evaluated for use in specific situations to determine the one(s) most applicable.

3.1 Comparisons of a Single-Plate Equation to a Double-Plate Equation

The "new" Cour-Palais double-plate penetration predictor equation is the only equation in this paper which covers all three phase changes of the projectile impacting the bumper plate, and was developed to predict damage due to both the meteoroid and orbital debris particle impacts. Therefore, it was selected to compare predicted ballistic limit particles to those predicted by the single-plate penetration equation to show the effectiveness of double-plate structures over single-plate structures. The "modified" Cour-Palais single-plate penetration predictor equation was selected for this comparison for consistency.[4] Microsoft® Excel software was used to complete the calculations. Projectiles are assumed spherical, and to have the properties of 2017 aluminum, impacting normal to the target surface. The material properties for the 2219–T87 aluminum alloy were used for both the single- and double-plate structures. The thickness of the single-plate was set to 0.200 in. (0.51 cm). For the double-plate structure, the thicknesses of the bumper plate and rear-wall plate were set to 0.050 in. (0.13 cm) and 0.150 in. (0.38 cm), to give a total thickness equal to that of the single plate (see fig. 2). Table 1 lists the ballistic limit projectile diameters predicted by the single- and double-plate penetration equations for the velocities ranging from 2 to 15 km/sec. Figure 3 shows the ballistic limit curves generated by the single- and double-plate penetration equations, a plot of the calculated ballistic limit particle diameters. The ballistic limit is the predicted projectile size for a given particle material, impact angle, and velocity, which will just completely penetrate the rear-wall plate of the double-plate structure. Any larger projectiles are expected to completely penetrate the rear-wall plate, and any projectiles smaller than the ballistic limit are not expected to completely penetrate.

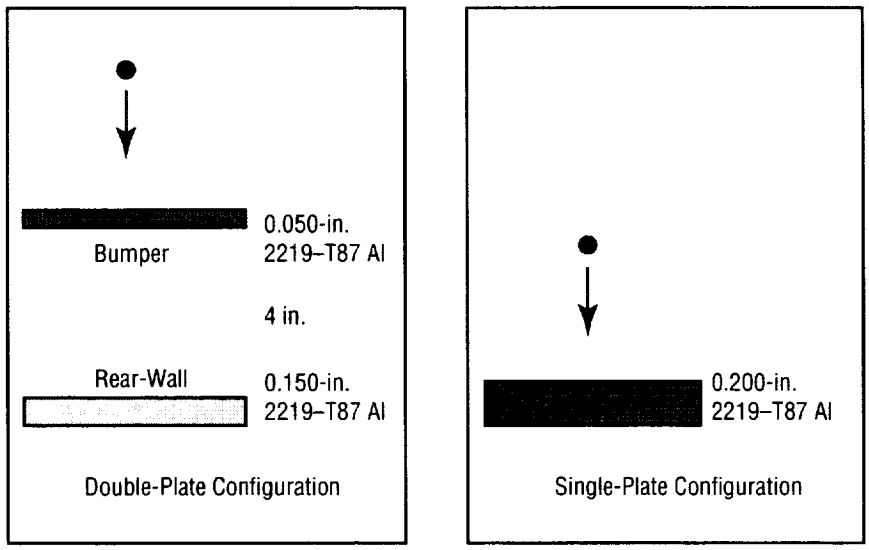

Figure 2. Single- and double-plate configurations compared.

Table 1. Projectile diameters predicted by the single- and double-plate penetration equations.

Impact Velocity (km/sec)	Projectile Diameter (cm)		Percent Difference
	Single-Plate	Double-Plate	
2	0.3651	0.3777	3.47
3	0.2826	0.2924	3.47
4	0.2356	0.3955	67.83
5	0.2047	0.4985	143.58
6	0.1824	0.6016	229.81
7	0.1655	0.7044	325.69
8	0.1521	0.6444	323.70
9	0.1412	0.5958	321.95
10	0.1321	0.5554	320.39
11	0.1244	0.5212	318.99
12	0.1177	0.4918	317.71
13	0.1119	0.4662	316.54
14	0.1068	0.4438	315.46
15	0.1023	0.4238	314.46

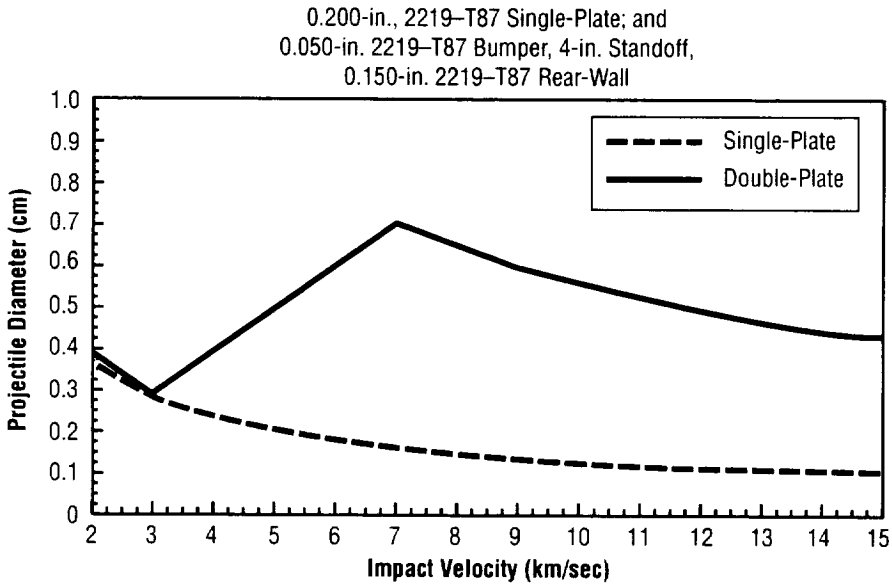

Figure 3. Ballistic limit curves generated by single- and double-plate penetration equations.

For the low-velocity range; i.e., from 2 to 3 km/sec, the projectiles are expected to penetrate through the bumper plate without shattering, melting, or vaporizing. Therefore, the double plate reacts similarly to the single-plate, resulting in nearly identical curves in figure 3. In this velocity range, the projectile sizes which the double-plate can stop are only 3.5 percent larger than the ones stopped by the single plate. For the intermediate-velocity range; i.e., from 3 to 7 km/sec, the bumper plate starts to shatter the projectile, creating many smaller particles, spreading their energy over a wider area of the rear-wall plate. The greater the velocity, the more smaller particles will be created by breaking the projectile, and the wider the area they are spread over the rear-wall plate. Therefore, the double-plate can stop much larger projectiles than the single-plate. The projectile sizes which the double-plate can stop range from 68 percent to over 300 percent larger than the ones the single-plate can stop. For the high-velocity range; i.e., >7 km/sec, the projectile starts to melt, then vaporize, after impacting the bumper plate. The projectile sizes which the double-plate can stop are over 300 percent larger than the ones the single-plate can stop. Many double-plate penetration equations were developed only for the high-velocity range, as discussed in section 2, since the environment of concern was meteoroids, with expected impact velocities >10 km/sec.

3.2 Comparisons of Double-Plate Penetration Equations

Microsoft Excel software was used to construct a spreadsheet to calculate the ballistic limit projectile diameters predicted by the seven double-plate penetration equations for velocities ranging from 2 to 15 km/sec. Predictions were made and plotted for three double-plate configurations shown in figure 4. These designs were chosen for this study because of the test database available from early Space Station debris shield development. Because these configurations are so similar, the differences between the results predicted by the double-plate penetration equations are small. Note, however, that configuration 2 will provide the highest resistance to penetration, due to increased spacing, even over the more massive configuration 3.

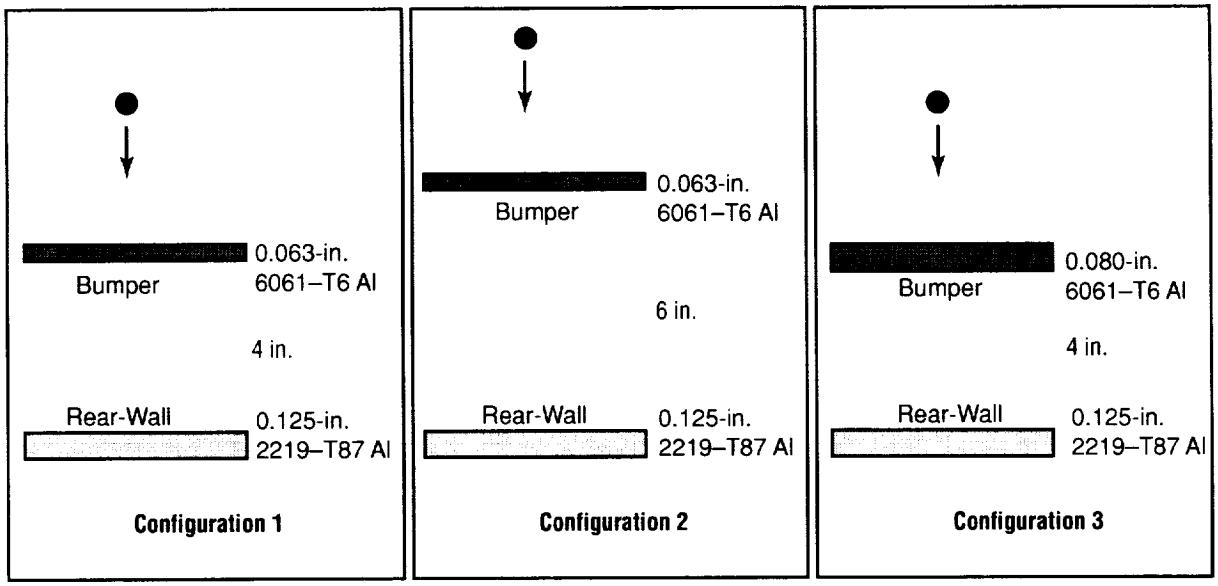

Figure 4. Three shield configurations used in the comparison of predictor equations to test data.

The ballistic limit projectile diameters predicted by the Nysmith and Wilkinson double-plate penetration equations for configuration 3 are shown in tables 2 and 3, respectively. Figures 5–7 show the ballistic limit curves generated by the seven double-plate penetration equations discussed in section 2 for each of these three cases.

Table 2. Ballistic limit projectile diameters predicted by the Nysmith double-plate penetration equation for configuration 3.

Nysmith penetration equation (developed with Pyrex glass projectiles simulating meteoroids, for impact velocities >6 km/sec)

					Ratio of t_b to t_w	
Bumper Thickness (t_b)	0.080	in.	0.2032	cm	39.02	%
Rear-Wall Thickness (t_w)	0.125	in.	0.3175	cm	60.98	%
Standoff	4.00	in.	10.16	cm		
Al Projectile Density	2.713	gm/cm^3	Pyrex Projectile Density		2.230	gm/cm^3

Impact Velocity (km/sec)	Calculated Diameter (cm)	Check 1 (t_b/d<0.5)	Check 2 (t_w/d<1)	Pyrex Projectile Diameter (cm)	Pyrex Projectile Diameter (in.)	Aluminum Projectile Diameter (cm)	Aluminum Projectile Diameter (in.)
6	0.7373	0.2756	0.4306	0.7373	0.2903	0.6906	0.2719
7	0.7265	0.2797	0.4370	0.7265	0.2860	0.6806	0.2679
8	0.7173	0.2833	0.4426	0.7173	0.2824	0.6720	0.2645
9	0.7093	0.2865	0.4476	0.7093	0.2793	0.6645	0.2616
10	0.7022	0.2894	0.4521	0.7022	0.2765	0.6578	0.2590
11	0.6959	0.2920	0.4562	0.6959	0.2740	0.6519	0.2566
12	0.6901	0.2944	0.4600	0.6901	0.2717	0.6465	0.2545
13	0.6849	0.2967	0.4636	0.6849	0.2696	0.6416	0.2526
14	0.6801	0.2988	0.4669	0.6801	0.2678	0.6371	0.2508
15	0.6756	0.3008	0.4699	0.6756	0.2660	0.6329	0.2492

Table 3. Ballistic limit projectile diameters predicted by the Wilkinson double-plate penetration equation for configuration 3.

Wilkinson penetration equation (projectile melt/vaporization predictor for impact velocities >8 km/sec)

	Density			Thickness		Thickness	
Projectile	2.713	gm/cm^3	Bumper	0.080	in.	0.2032	cm
Bumper	2.713	gm/cm^3	Rear-Wall	0.125	in.	0.3175	cm
Rear-Wall	2.851	gm/cm^3	Standoff	4.00	in.	10.160	cm

Rear-Wall Material Constant: 0.401 Penetration Resistance (L_2)

Impact Velocity (km/sec)	Case 1 Calculated Diameter (cm)	Case 1 Check 1 ($dr_p/r_bt_b>1$)	Case 2 Calculated Diameter (cm)	Case 2 Check 2 ($dr_p/r_bt_b<1$)	Al Projectile Diameter by Original Wilkinson (cm)	Al Projectile Diameter by Original Wilkinson (in.)	Al Projectile Diameter by Modified Wilkinson (0.8 × Original Wilkinson) (cm)	Al Projectile Diameter by Modified Wilkinson (0.8 × Original Wilkinson) (in.)
8	0.9908	4.8760	1.6801	–	0.9908	0.3901	0.7926	0.3121
9	0.9621	4.7345	1.6154	–	0.9621	0.3788	0.7696	0.3030
10	0.9370	4.6115	1.5597	–	0.9370	0.3689	0.7496	0.2951
11	0.9150	4.5029	1.5109	–	0.9150	0.3602	0.7320	0.2882
12	0.8953	4.4060	1.4677	–	0.8953	0.3525	0.7162	0.2820
13	0.8776	4.3187	1.4291	–	0.8776	0.3455	0.7020	0.2764
14	0.8614	4.2394	1.3942	–	0.8614	0.3392	0.6892	0.2713
15	0.8467	4.1669	1.3625	–	0.8467	0.3334	0.6774	0.2667

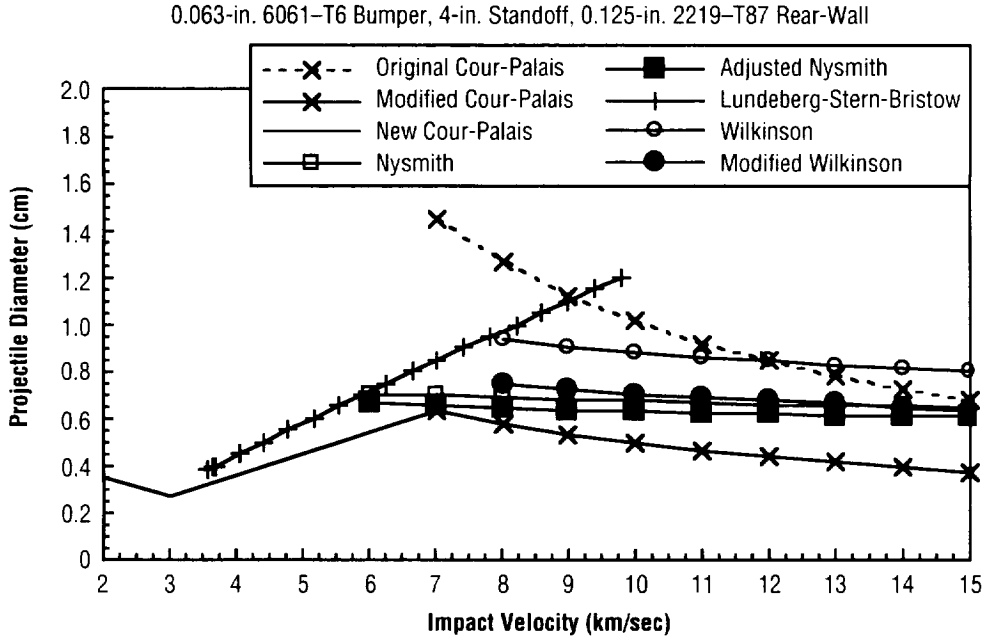

Figure 5. Ballistic limit curves generated by the double-plate penetration equations for configuration 1.

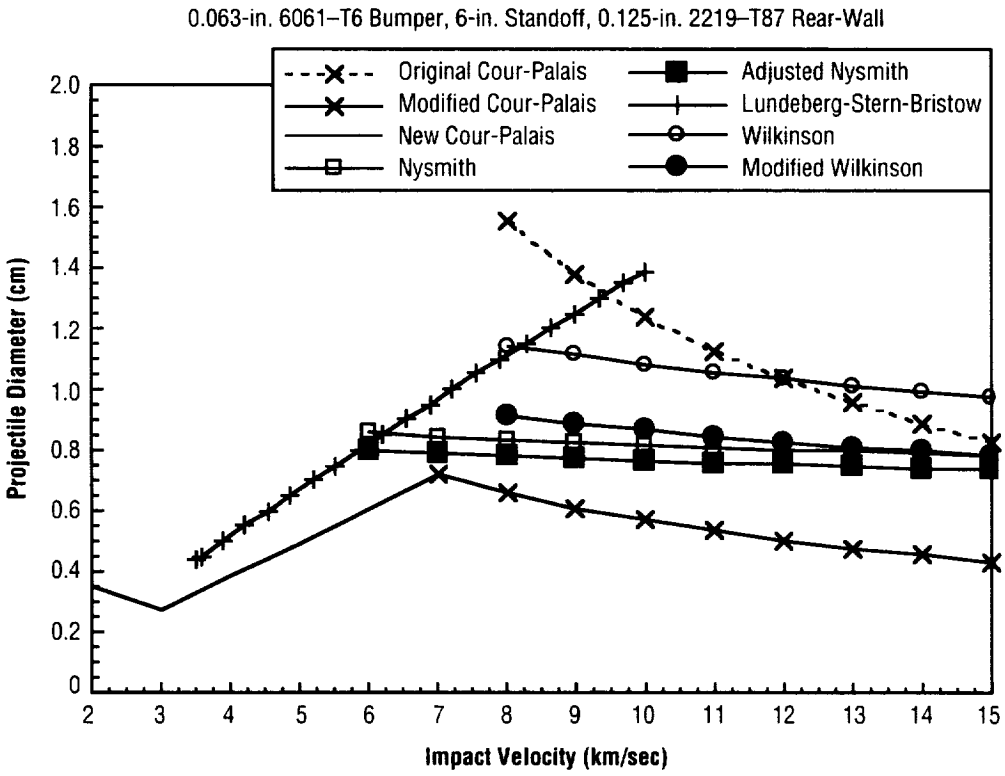

Figure 6. Ballistic limit curves generated by the double-plate penetration equations for configuration 2.

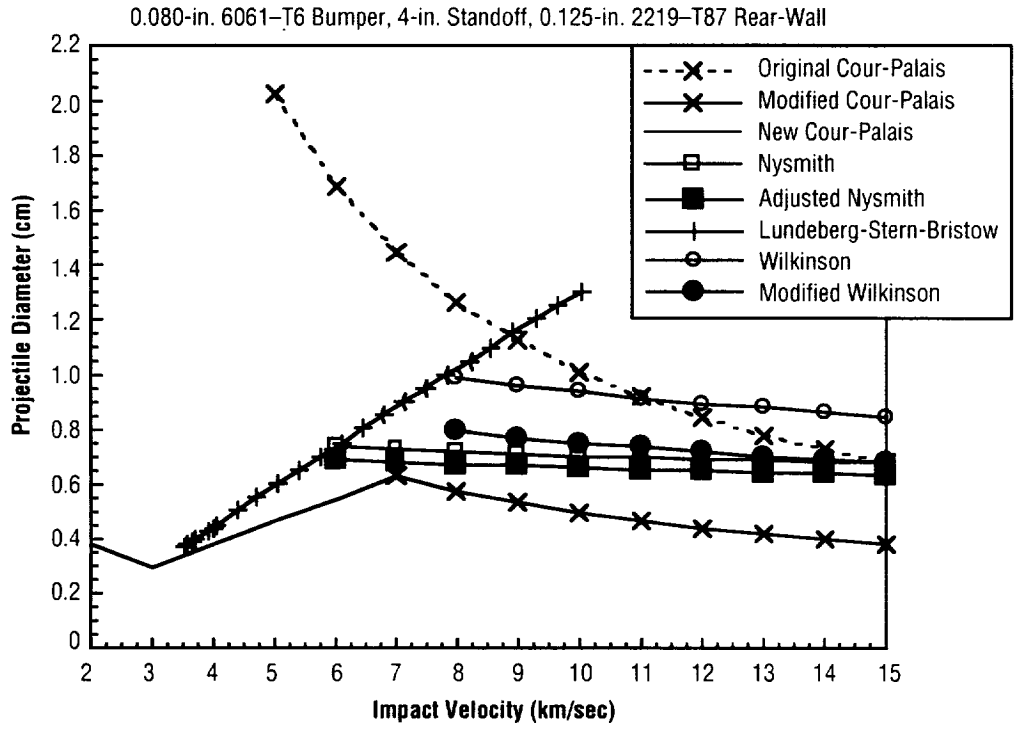

Figure 7. Ballistic limit curves generated by the double-plate penetration equations for configuration 3.

The ballistic limit projectile diameters predicted in this study by the Nysmith equation were "scaled" from Pyrex glass to aluminum projectile diameters to estimate the change in penetration capability due to projectile material density. This is an estimation method used at MSFC, not one used by or recommended by Nysmith or any other of the developers of the double-plate predictors in this study.

As discussed earlier in this report, all the double-plate penetration equations except the Wilkinson equation were derived from test results with impact velocities as high as 9 km/sec. These penetration equations were extrapolated to predict the projectile diameters for velocities >9 km/sec. The Wilkinson equation was developed using the equations of linear plate theory with simplifying assumptions concerning the plate's reaction in the vaporization region. Therefore, the projectile diameters predicted by these equations have not been verified by experiment. Currently, there are a few facilities which can launch projectiles to velocities up to 12 km/sec. These tests can be very expensive and offer less confidence in the test results than those accomplished at <9 km/sec. In conjunction with tests >9 km/sec, hydrocode analyses can provide more confidence in the predictor equations.

Figures 5–7 illustrate the ballistic limit curves generated by the seven double-plate penetration equations for the three double-plate structures in this study. Only the new Cour-Palais equation is applicable in the low-velocity range. Two penetration equations are applicable in the intermediate-velocity range, the new Cour-Palais and the Lundeberg-Stern-Bristow equations. For the high-velocity range, the most conservative penetration equations are the modified and new Cour-Palais equations. Also for the high-velocity range, the least conservative penetration equations are the original Cour-Palais equation for the velocities <11–12 km/sec and the Wilkinson equation for the velocities >11–12 km/sec. The Nysmith, adjusted Nysmith, and modified Wilkinson equations predicted the projectile sizes which fell between the most and least conservative equations. It is interesting to note that the projectile sizes predicted by these three equations are similar, considering their varying development parameters.

For configuration 1, the projectile sizes predicted by the Lundeberg-Stern-Bristow equation are between 22 and 35 percent larger than those by the new Cour-Palais equation. At 8 km/sec, the projectile size predicted by the least conservative equation is 120 percent larger than the one by the most conservative equation. At 15 km/sec, the projectile size predicted by the least conservative equation is 111 percent larger than the one by the most conservative equation. The projectile sizes predicted by the modified Wilkinson equation are between 5 and 16 percent larger than those by the adjusted Nysmith equation. The projectile sizes predicted by the modified Wilkinson equation are between 30 and 69 percent larger than those by the modified and new Cour-Palais equations. Finally, the projectile sizes predicted by the original Cour-Palais equation are between 6 and 69 percent larger than those by the modified Wilkinson equation.

For configuration 2, the projectile sizes predicted by the Lundeberg-Stern-Bristow equation are 34.5 percent larger than those by the new Cour-Palais equation, in the intermediate-velocity range. At 8 km/sec, the projectile size predicted by the least conservative equation is 136 percent larger than the one by the most conservative equation. At 15 km/sec, the projectile size predicted by the least conservative equation is 126 percent larger than the one by the most conservative equation. The projectile sizes predicted by the modified Wilkinson equation are between 6 and 17 percent larger than those by the adjusted Nysmith equation. The projectile sizes predicted by the modified Wilkinson equation are between 39 and 81 percent larger than those by the modified and new Cour-Palais equations. Finally, the

projectile sizes predicted by the original Cour-Palais equation are between 6 and 69 percent larger than those by the modified Wilkinson equation.

For configuration 3, in the intermediate-velocity range, the projectile sizes predicted by the Lundeberg-Stern-Bristow equation are between 17 and 40 percent larger than those predicted by the new Cour-Palais equation. At 8 km/sec, the projectile size predicted by the least conservative equation is 120 percent larger than the one by the most conservative equation. At 15 km/sec, the projectile size predicted by the least conservative equation is 124 percent larger than the one by the most conservative equation. The projectile sizes predicted by the modified Wilkinson equation are between 7 and 18 percent larger than those by the adjusted Nysmith equation. The projectile sizes predicted by the modified Wilkinson equation are between 38 and 79 percent larger than those by the modified and new Cour-Palais equations. Finally, at 8 km/sec, the projectile size predicted by the original Cour-Palais equation is 60 percent larger than the one by the modified Wilkinson equation. However, at 15 km/sec, the projectile size predicted by the modified Wilkinson equation is only 0.4 percent larger than the one predicted by the original Cour-Palais equation.

3.3 Comparisons With Test Results

Several hundred HVI tests, including the double-plate structures were performed at MSFC during the development of the M/OD shield design for the *International Space Station* (*ISS*) program. The results from 58 of these tests, shown in table 4, were used in this study to compare with predictor equation results for configurations 1–3.

Table 4. Hypervelocity impact test results from the *ISS* program.

Test Number	Impact Velocity (km/sec)	Projectile			Bumper		Standoff Distance (in.)	Rear-Wall		
		Material	Diameter (in.)	Diameter (cm)	Material	Thickness (in.)		Material	Thickness (in.)	Pen. (Y/N)
SS-P-028	3.00	1100 Al	0.125	0.3175	6061-T6	0.063	4	2219-T87	0.125	N
SS-P-027A	3.87	1100 Al	0.187	0.4750	6061-T6	0.063	4	2219-T87	0.125	Y
SS-P-027B	4.15	1100 Al	0.187	0.4750	6061-T6	0.063	4	2219-T87	0.125	Y
SS-P-027	4.53	1100 Al	0.187	0.4750	6061-T6	0.063	4	2219-T87	0.125	N
SS-P-001	2.75	1100 Al	0.250	0.6350	6061-T6	0.063	4	2219-T87	0.125	Y
SS-P-002	2.99	1100 Al	0.250	0.6350	6061-T6	0.063	4	2219-T87	0.125	Y
SS-148C	3.63	1100 Al	0.250	0.6350	6061-T6	0.063	4	2219-T87	0.125	Y
SS-PT4A	3.64	1100 Al	0.250	0.6350	6061-T6	0.063	4	2219-T87	0.125	Y
SS-PT4B	4.26	1100 Al	0.250	0.6350	6061-T6	0.063	4	2219-T87	0.125	Y
SS-P-003	4.90	1100 Al	0.250	0.6350	6061-T6	0.063	4	2219-T87	0.125	Y
SS-P-004	4.95	1100 Al	0.250	0.6350	6061-T6	0.063	4	2219-T87	0.125	Y
SS-148A	5.74	1100 Al	0.250	0.6350	6061-T6	0.063	4	2219-T87	0.125	N
EHSS-2B	5.88	1100 Al	0.250	0.6350	6061-T6	0.063	4	2219-T87	0.125	Y
SS-P-034B	7.06	1100 Al	0.250	0.6350	6061-T6	0.063	4	2219-T87	0.125	Y
SS-P-022	5.09	1100 Al	0.262	0.6655	6061-T6	0.063	4	2219-T87	0.125	Y
SS-P-022B	6.89	1100 Al	0.262	0.6655	6061-T6	0.063	4	2219-T87	0.125	Y
SS-P-021A	6.47	1100 Al	0.300	0.7620	6061-T6	0.063	4	2219-T87	0.125	Y
SS-P-021	6.63	1100 Al	0.300	0.7620	6061-T6	0.063	4	2219-T87	0.125	Y
SS-T2-8	3.39	1100 Al	0.313	0.7950	6061-T6	0.063	4	2219-T87	0.125	Y
SS-PT8A	4.35	1100 Al	0.313	0.7950	6061-T6	0.063	4	2219-T87	0.125	Y
SS-PT8B	4.37	1100 Al	0.313	0.7950	6061-T6	0.063	4	2219-T87	0.125	Y
SS-T2-6A	4.64	1100 Al	0.313	0.7950	6061-T6	0.063	4	2219-T87	0.125	Y
EHSS-6C	6.64	1100 Al	0.313	0.7950	6061-T6	0.063	4	2219-T87	0.125	Y
EH3-A	6.64	1100 Al	0.313	0.7950	6061-T6	0.063	4	2219-T87	0.125	Y
EH4-B	6.76	1100 Al	0.313	0.7950	6061-T6	0.063	4	2219-T87	0.125	Y
SS-T2-18	5.05	1100 Al	0.375	0.9525	6061-T6	0.063	4	2219-T87	0.125	Y
SS-P-015	2.85	1100 Al	0.125	0.3175	6061-T6	0.063	6	2219-T87	0.125	N
SS-P-015C	3.01	1100 Al	0.125	0.3175	6061-T6	0.063	6	2219-T87	0.125	N
SS-P-014D	3.26	1100 Al	0.187	0.4750	6061-T6	0.063	6	2219-T87	0.125	Y
SS-P-014	3.72	1100 Al	0.187	0.4750	6061-T6	0.063	6	2219-T87	0.125	Y
SS-P-014A	4.18	1100 Al	0.187	0.4750	6061-T6	0.063	6	2219-T87	0.125	Y
SS-P-013	4.77	1100 Al	0.250	0.6350	6061-T6	0.063	6	2219-T87	0.125	Y
SS-P-013C	5.79	1100 Al	0.250	0.6350	6061-T6	0.063	6	2219-T87	0.125	Y
SS-P-020C	6.63	1100 Al	0.300	0.7620	6061-T6	0.063	6	2219-T87	0.125	Y
SS-T2-20	4.73	1100 Al	0.313	0.7950	6061-T6	0.063	6	2219-T87	0.125	Y
SS-P-035	6.69	1100 Al	0.350	0.8890	6061-T6	0.063	6	2219-T87	0.125	Y
SS-P-025B	2.25	6061-T6 Al	0.187	0.4750	6061-T6	0.063	6	2219-T87	0.125	Y
SS-P-025C	2.59	6061-T6 Al	0.187	0.4750	6061-T6	0.063	6	2219-T87	0.125	N
SS-P-025A	3.27	6061-T6 Al	0.187	0.4750	6061-T6	0.063	6	2219-T87	0.125	N
SS-P-025	3.71	6061-T6 Al	0.187	0.4750	6061-T6	0.063	6	2219-T87	0.125	N
SS-P-024C	5.80	6061-T6 Al	0.250	0.6350	6061-T6	0.063	6	2219-T87	0.125	Y
SS-P-024F	5.88	6061-T6 Al	0.250	0.6350	6061-T6	0.063	6	2219-T87	0.125	Y
SS-P-018RV	7.12	6061-T6 Al	0.262	0.6655	6061-T6	0.063	6	2219-T87	0.125	Y
SS-P-016	5.14	6061-T6 Al	0.300	0.7620	6061-T6	0.063	6	2219-T87	0.125	Y
SS-P-016A	6.04	6061-T6 Al	0.300	0.7620	6061-T6	0.063	6	2219-T87	0.125	Y
SS-P-016B	6.33	6061-T6 Al	0.300	0.7620	6061-T6	0.063	6	2219-T87	0.125	Y
SS-P-016C	6.63	6061-T6 Al	0.300	0.7620	6061-T6	0.063	6	2219-T87	0.125	Y
SS-P-016E	6.78	6061-T6 Al	0.300	0.7620	6061-T6	0.063	6	2219-T87	0.125	Y
SS-190D	2.00	1100 Al	0.187	0.4750	6061-T6	0.080	4	2219-T87	0.125	N
SS-101	3.09	1100 Al	0.187	.0.4750	6061-T6	0.080	4	2219-T87	0.125	Y
SS-109B	3.61	1100 Al	0.187	0.4750	6061-T6	0.080	4	2219-T87	0.125	N
SS-101A	3.70	1100 Al	0.187	0.4750	6061-T6	0.080	4	2219-T87	0.125	Y
SS-109A	4.06	1100 Al	0.187	0.4750	6061-T6	0.080	4	2219-T87	0.125	N
SS-101B	4.27	1100 Al	0.187	0.4750	6061-T6	0.080	4	2219-T87	0.125	Y
SS-109	7.39	1100 Al	0.187	0.4750	6061-T6	0.080	4	2219-T87	0.125	N
SS-102	7.20	1100 Al	0.300	0.7620	6061-T6	0.080	4	2219-T87	0.125	Y
SS-107A	6.74	1100 Al	0.350	0.8890	6061-T6	0.080	4	2219-T87	0.125	Y
SS-107B	6.82	1100 Al	0.350	0.8890	6061-T6	0.080	4	2219-T87	0.125	Y

A total of 26 tests were performed using configuration 1 (0.063-in. 6061–T6 bumper, 4-in. standoff, 0.125-in. 2219–T87 rear-wall double-plate structure). The 1100 aluminum projectile diameters ranged from 0.32 cm (0.125 in.) to 0.95 cm (0.375 in.), and the projectile velocities ranged from 2.75 to 7.06 km/sec. For configuration 2 (0.063-in. 6061–T6 bumper, 6-in. standoff, 0.125-in. 2219–T87 rear-wall double-plate structure), 22 tests were performed. The 1100 and 6061–T6 aluminum projectile diameters ranged from 0.32 cm (0.125 in.) to 0.89 cm (0.350 in.), and the projectile velocities ranged from 2.25 to 7.12 km/sec. Finally, 10 tests were performed using configuration 3 (0.080-in. 6061–T6 bumper, 4-in. standoff, 0.125-in. 2219–T87 rear-wall double-plate structure). The 1100 aluminum projectile diameters ranged from 0.48 cm (0.187 in.) to 0.89 cm (0.350 in.), and the projectile velocities ranged from 2 to 7.39 km/sec. Figures 8–10 show the ballistic limit curves generated by the double-plate penetration equations with the test results for the three configurations.

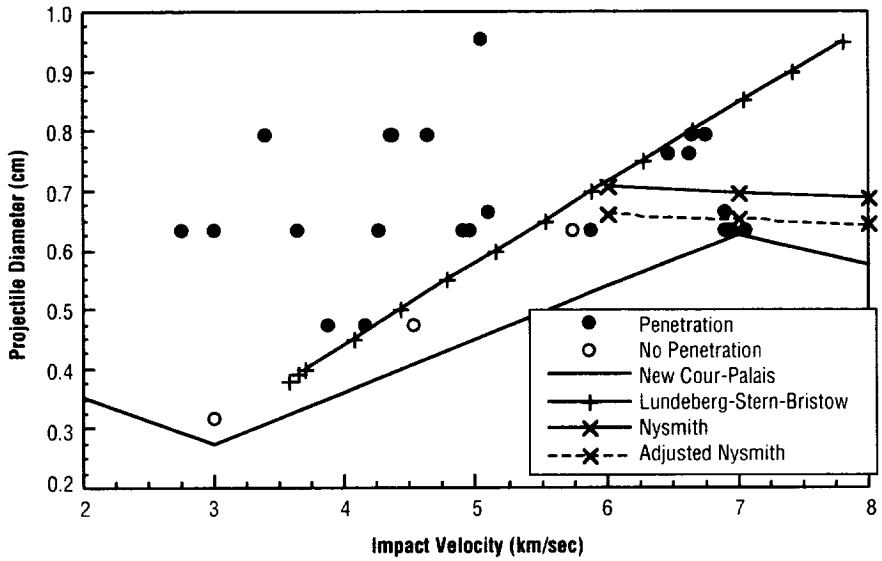

Figure 8. Comparisons of the double-plate penetration equations with the test results for configuration 1.

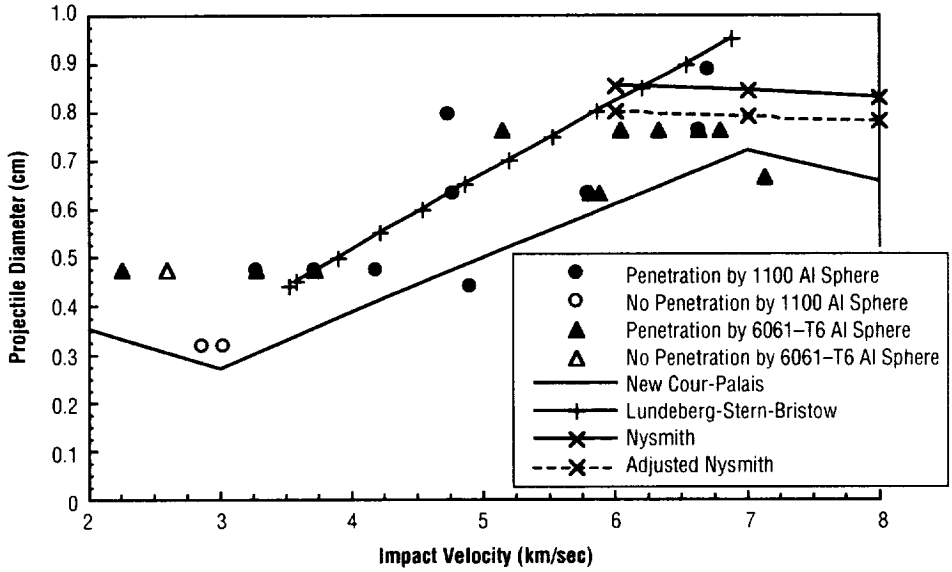

Figure 9. Comparisons of the double-plate penetration equations with the test results for configuration 2.

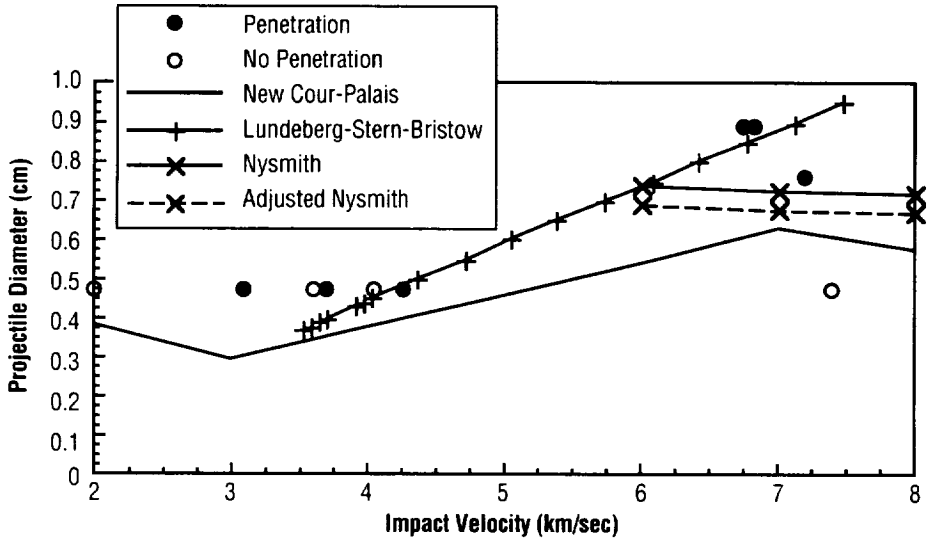

Figure 10. Comparisons of the double-plate penetration equations with the test results for configuration 3.

Figure 8 shows the ballistic limit curves generated by the double-plate penetration equations for configuration 1. Only 3 of the 26 tests resulted in no perforation of the rear-wall plate. Test No. SSP028 at 3 km/sec, showed that a 0.3175-cm projectile did not perforate the rear-wall plate. Conservatively, the new Cour-Palais equation predicted that the 0.2729-cm projectile traveling at the same velocity would perforate the rear-wall plate, a 16 percent smaller diameter projectile. Test No. SS–P–027 showed that a 0.475-cm projectile traveling at 4.53 km/sec did not perforate the rear-wall plate. The new Cour-Palais equation again conservatively predicted that the 0.4085-cm projectile traveling at the same velocity would perforate the rear-wall plate. Perhaps more realistically, the Lundeberg-Stern-Bristow equation predicted that a 0.5149-cm projectile traveling at the same velocity would perforate the rear-wall plate. Finally, test No. SS–148A showed that a 0.635-cm projectile traveling at 5.74 km/sec did not perforate the rear-wall plate, and test No. EHSS–2B showed that the same size projectile traveling at 5.88 km/sec did perforate the rear-wall plate, indicating a ballistic limit point for the 0.635-cm projectile should lie between these two velocities. The new Cour-Palais equation again conservatively predicted that a 0.5158-cm projectile traveling at 5.74 km/sec would perforate the rear-wall plate, a 23 percent smaller projectile than the one tested. More in line with the data, the Lundeberg-Stern-Bristow equation predicted that a 0.679-cm projectile traveling at the same velocity would perforate the rear-wall plate.

To summarize, when comparing to data for configuration 1, the new Cour-Palais equation more accurately predicted rear-wall perforation for velocities >6 km/sec. The Lundeberg-Stern-Bristow equation was a better predictor between 4 and 6 km/sec. However, the Nysmith and adjusted Nysmith equations did not predict correctly.

Figure 9 shows the ballistic limit curves generated by the double-plate penetration equations with the test results for configuration 2. Five of the twenty-two tests resulted in no perforation of the rear-wall plate. Of test Nos. SS–P–015 and SS–P–015C, both with 0.3175-cm projectiles; at 2.85 and 3.01 km/sec, respectively, neither perforated the rear-wall plate. The new Cour-Palais equation underpredicted the ballistic limit projectile, indicating that a 0.2729-cm projectile traveling at 3 km/sec would perforate the rear-wall plate, a 16 percent smaller projectile than the one in the tests. At slightly higher velocities, results of test Nos. SS–P–025A and SS–P–025 showed that 0.475-cm diameter 6061–T6 projectiles

traveling at 3.27 and 3.71 km/sec, respectively, could not perforate the rear-wall plate. However, the same size 1100 projectiles (test Nos. SS–P–014D and SS–P–014) at 3.26 and 3.72 km/sec did perforate the rear-wall plate. These test results indicate that the ballistic limit for configuration 2 is reached near these velocities for a 0.475-cm aluminum projectile. Again, the new Cour-Palais equation predicted that the rear-wall plate would be perforated by a projectile smaller than those in the tests, a 0.3019-cm projectile traveling at 3.26 km/sec and a 0.352-cm projectile traveling at 3.71 km/sec, respectively. For the tests performed at velocities between 4 and 7 km/sec, the new Cour-Palais equation predicted correctly, although there were no "no perforation" results to compare with in this velocity range. Contrary to earlier comparisons, the new Cour-Palais equation predicted that a 0.7099-cm projectile at 7.12 km/sec was required to perforate the rear-wall plate, a larger projectile than the 0.6655-cm projectile that perforated in test No. SS–018RV. The Lundeberg-Stern-Bristow, Nysmith, and adjusted Nysmith equations all predicted higher ballistic limit projectiles than the tests results for configuration 2.

Figure 10 shows the ballistic limit curves generated by the double-plate penetration equations with the test results for configuration 3. Four of the ten tests resulted in no perforation of the rear-wall plate. The results of test No. SS–190D showed that the rear-wall plate stopped a 0.475-cm projectile traveling at 2 km/sec. However, the new Cour-Palais equation predicted that the rear-wall plate would be perforated by a smaller 0.3802-cm projectile traveling at the same velocity, a 25 percent smaller projectile than the one tested. Test results showed that the rear-wall plate stopped a 0.475-cm projectile traveling at 3.61 km/sec (test No. SS–109B), but could not stop the same size projectile traveling at 3.70 km/sec (test No. SS–101A). At 3.61 km/sec, both the new Cour-Palais equation and the Lundeberg-Stern-Bristow equation predicted smaller ballistic limit projectiles of 0.3451 cm (38 percent smaller) and 0.3864 cm (23 percent smaller), respectively. For velocities >6 km/sec, the new Cour-Palais, Nysmith, and adjusted Nysmith equations predicted correctly.

3.4 Shield Design Considerations

Before choosing a debris shield design, several details of the design must be considered. In addition to the obvious shield material and thickness selections, careful reflection must be given to the benefits of simplicity of a single-plate design over increased shield effectiveness with a multiple-plate design. Increased shield effectiveness inevitably leads to increased mass. However, the designer can be resourceful in distributing the mass to maximize shield effectiveness for the spacecraft. Often the final design decision becomes one of how "safe" the project manager wants his/her vehicle to be, given a maximum allowable shield mass.

The designer can save much mass unwisely by choosing the least conservative equation, which underestimates the value for the perforating projectile diameter. Therefore, he/she can reduce the cost significantly, but this choice could result in unforeseen critical damage to the spacecraft or loss of the entire spacecraft. On the other hand, the designer can design a conservative, well-protected spacecraft but the spacecraft could become very heavy, increasing launch and material costs significantly. A thorough understanding of all the factors involved in designing spacecraft shielding can help the designer choose the most effective design for the least mass.

3.4.1 Single-Versus Double-Plate Shielding

It is not good design practice to include only the masses of the walls themselves when deciding between single- and double-plate shielding. A design comparison should also include the masses of additional support structure required for the double-plate design. As an example, an unverified estimate of this additional mass from the Space Station shield design is 8 percent of the mass of the "shield" itself. Using this estimate to recalculate the example from section 3.1: if the support structure mass of the double-plate design is estimated as 8 percent of the mass of the two plates, then the total mass per unit area of the shield in the example would increase from 0.0204 to 0.0220 lb/in^2. Then an equal mass single-plate structure would be 0.216 in. (0.55 cm) thick. Table 5 shows the comparison between these two shields, with corresponding percent differences in ballistic limit projectile sizes. The percent difference between the double- and single-plate shields has decreased; the double-plate shield is slightly less advantageous than it previously was. For this particular case, even including the mass of the additional hardware, the double-plate shield remains a superior shield design over the single-plate shield. In some instances the mass of the suppport structure will be excessive.

Table 5. Projectile diameters predicted for the single-plate shield with additional mass compared to the double-plate shield.

Impact Velocity (km/sec)	Projectile Diameter (cm)		Percent Difference
	Single-Plate	Double-Plate	
2	0.3927	0.3777	-3.80
3	0.3040	0.2924	-3.80
4	0.2535	0.3955	56.03
5	0.2201	0.4985	126.46
6	0.1962	0.6016	206.62
7	0.1780	0.7044	295.76
8	0.1636	0.6444	293.91
9	0.1519	0.5958	292.28
10	0.1421	0.5554	290.83
11	0.1338	0.5212	289.53
12	0.1266	0.4918	288.34
13	0.1204	0.4662	287.25
14	0.1149	0.4438	286.25
15	0.1100	0.4238	285.31

The ballistic limit curves for this example are shown in figure 11. Notice that the single-plate shield now has improved performance over the double-plate at very low velocities where the projectile remains intact. Also, with the 8-percent increase in shield mass, the single-plate shield can stop projectiles ≈7.5 percent larger in diameter over all three velocity ranges, than the shield without the additional mass.

3.4.2 Increased Spacing

As noted in section 3.2, increased spacing between plates of shielding can be more beneficial than increased plate thicknesses. There are limits to the effectiveness of increased spacing, dependent upon both impact physics and the increasing mass of the support structure. The support structure mass cannot be discounted in the design selection. Also, in many situations space is limited by allowable payload envelope within a launch vehicle. These requirements must all be traded to determine the most effective, mass-efficient shield design.

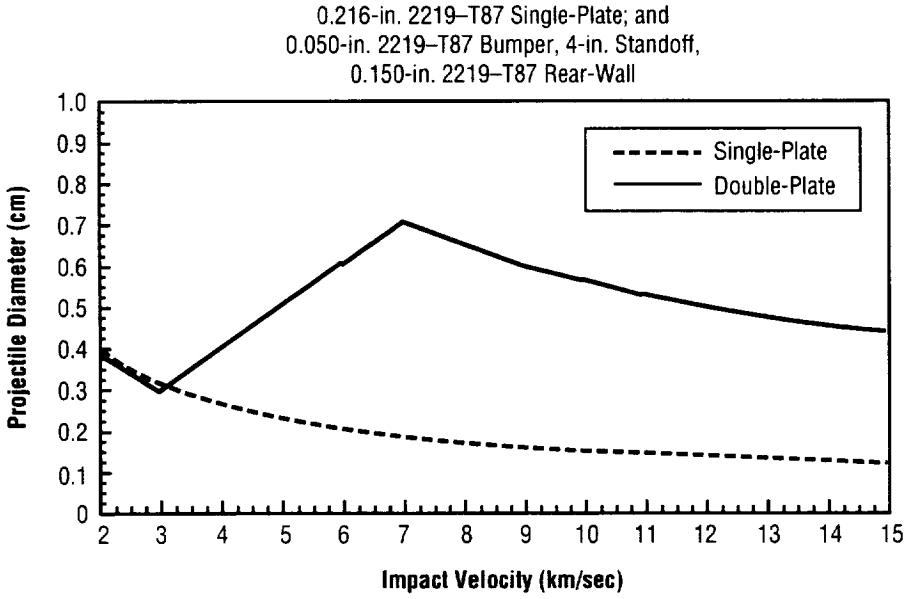

Figure 11. Ballistic limit curves for the double-plate and increased thickness single-plate configurations.

3.4.3 Smart Mass Distribution

Different spacecraft components are vulnerable to the M/OD environment in varying degrees. Rather than try to cover an entire spacecraft in the same shield design, the clever designer will examine individual components and design separate shields to meet the needs of each component. In this way, the allotted mass for shielding can be used only for those most vulnerable items. Some may require only a single-plate shield while others, such as high-pressure fuel bottles, may require multiplate shielding. Remember to combine all the components' probabilities of penetration to quantify the overall spacecraft vulnerability to projectile impact. The individual components' probabilities of penetration are just that—individual.

4. RECOMMENDATIONS/CONCLUSIONS

It is very difficult to choose the "right" ballistic limit prediction equation to use for all cases. The shield analyst/designer must choose the equation most applicable to his/her specific design, by comparing HVI test results of the design to the results predicted by the equations. Even though most of these double-plate penetration equations are empirically developed with various materials and configurations, there can be no confidence in the shield design produced by these equations without verification by tests. The shields designed with these equations should be tested with the actual configurations and materials, at realistic velocities with appropriate projectile materials, to prove the design will act as predicted when impacted by a meteoroid or orbital debris particle. Only then can the design be declared acceptable for operations in LEO.

Only one penetration equation; i.e., the new Cour-Palais equation, was studied in this report for the low-velocity range. Others do exist, and are actively used in defense-related work; however, there are very few expected M/OD impacts in this velocity range. If predictions are needed for the low-velocity range, the single-plate penetration equations could be used instead of the double-plate penetration equations since the double-plate structure behaves very much like a single-plate structure in this range.

Two penetration equations; i.e., the new Cour-Palais and Lundeberg-Stern-Bristow equations, were studied for the intermediate-velocity range.

Four penetration equations and three modifications of these were studied for the high-velocity range. They predict a wide range of projectile diameters in this range, where the impact velocities of most of the meteoroid and orbital debris particles are expected to occur in LEO. Selection of the appropriate equation is most difficult for this range, due to the scarcity of directly applicable test data. Hydrocodes and inhibited shaped charge tests are often used as sources of checking for accuracy of the predictors in the high-velocity range. For the Space Station shield design, the most applicable equation in this range was found to be the modified Wilkinson equation.

When designing M/OD shields, simplicity of design is often preferred. Increased benefits of double-plate shields must be carefully considered with the increased spacing and support structure required and the increased design complexity. The designer can be resourceful in distributing different shield designs, both single-plate and multiplate designs, over individual spacecraft components, maximizing shield effectiveness while minimizing mass. Often the final shield design decision becomes one of how "safe" the project manager wants his/her vehicle to be, given a maximum allowable shield mass.

REFERENCES

1. Anderson, B.J.; and Smith, R.E.: "Natural Orbital Environment Guidelines for Use in Aerospace Vehicle Development." *NASA TM 4527*, 1994.

2. "Policy for Limiting Orbital Debris Generation." *NASA Management Instruction (NMI) 1700.8*, April 1993.

3. "Guidelines and Assessment Procedure for Limiting Orbital Debris." *NASA Safety Standard (NSS) 1740.14*, August 1995.

4. Hayashida, K.B.; and Robinson, J.H.: "Single Wall Penetration Equations." *NASA TM–103565*, 1991.

5. Whipple, F.L.: "Meteorites and Space Travel." *The Astronomical Journal*, Vol. 52, No. 1161, p.131, 1947.

6. Cour-Palais, B.G.: "Meteoroid Protection by Multiwall Structures." *AIAA Paper No. 69–372*, 1969.

7. Christiansen, E.L.: "Shield Sizing Equations." *NASA JSC Memorandum SN3–90–121*, October 12, 1990.

8. Christiansen, E.L.: "Whipple Shield Sizing Equations." *NASA JSC Memorandum SN3–91–19*, December 18, 1990.

9. Christiansen, E.L.: "Performance Equations for Advanced Orbital Debris Shields." *AIAA Paper No. 92–1462*, 1992.

10. Christiansen, E.L.: "Ballistic Limit Equations." *NASA JSC Memorandum SN3–91–21*, December 21, 1990.

11. Christiansen, E.L.: "Design and Performance Equations for Advanced Meteoroid and Debris Shield." *Int. J. Impact Engng*, Vol. 14., pp.145–156, 1993.

12. Nysmith, C.R.; and Summers, J.L.: "An Experimental Investigation of the Impact Resistance of Double-Sheet Structures at Velocities to 24,000 Feet Per Second." *NASA TN D–1431*, 1962.

13. Nysmith, C.R.: "An Experimental Impact Investigation of Aluminum Double-Sheet Structures." *AIAA Paper No. 69–375*, 1969.

14. Lundeberg, J.F.; Stern, P.H.; and Bristow, R.J.: "Meteoroid Protection for Spacecraft Structures." *NASA CR–54201*, 1965.

15. Burch, G.T.: "Multiplate-Damage Study." *Air Force Armament Laboratory Technical Report AFATL-TR-67-116*, 1967.

16. Madden, R.: "Ballistic Limit of Double-Walled Meteoroid Bumper Systems." *NASA TN D-3916*, 1967.

17. Wilkinson, J.P.D.: "A Penetration Criterion for Double-Walled Structures Subject to Meteoroid Impact." *AIAA Journal*, Vol. 7. No. 10, 1969.

18. Elfer, N.C.: "Structural Damage Prediction and Analysis for Hypervelocity Impacts—Handbook." *NASA CR-4706*, 1996.

19. Elfer, N.C.: "Space Debris and Meteoroid Protection." *Martin Marietta IR&D Report 826-2307*, 1988.

20. Abbott, R.D.; and Bjorkman, M.D.: "Momentum Transfer in the One-Dimensional Impact of Spaced Plates." *Proceedings of the APS 1991 Topical Conference on Shock Compression on Condensed Matter*, 1991.

REPORT DOCUMENTATION PAGE

Form Approved
OMB No. 0704-0188

1. AGENCY USE ONLY *(Leave Blank)*	2. REPORT DATE	3. REPORT TYPE AND DATES COVERED
	February 2000	Technical Memorandum

4. TITLE AND SUBTITLE

Double-Plate Penetration Equations

5. FUNDING NUMBERS

6. AUTHORS

K.B. Hayashida and J.H. Robinson

7. PERFORMING ORGANIZATION NAMES(S) AND ADDRESS(ES)

George C. Marshall Space Flight Center
Marshall Space Flight Center, AL 35812

8. PERFORMING ORGANIZATION REPORT NUMBER

M–962

9. SPONSORING/MONITORING AGENCY NAME(S) AND ADDRESS(ES)

National Aeronautics and Space Administration
Washington, DC 20546–0001

10. SPONSORING/MONITORING AGENCY REPORT NUMBER

NASA/TM—2000–209907

11. SUPPLEMENTARY NOTES

Prepared by Structures, Mechanics, and Thermal Department,
Engineering Directorate

12a. DISTRIBUTION/AVAILABILITY STATEMENT

Unclassified–Unlimited
Subject Category 39
Nonstandard Distribution

12b. DISTRIBUTION CODE

13. ABSTRACT *(Maximum 200 words)*

This report compares seven double-plate penetration predictor equations for accuracy and effectiveness of a shield design. Three of the seven are the Johnson Space Center original, modified, and new Cour-Palais equations. The other four are the Nysmith, Lundeberg-Stern-Bristow, Burch, and Wilkinson equations. These equations, except the Wilkinson equation, were derived from test results, with the velocities ranging up to 8 km/sec. Spreadsheet software calculated the projectile diameters for various velocities for the different equations. The results were plotted on projectile diameter versus velocity graphs for the expected orbital debris impact velocities ranging from 2 to 15 km/sec. The new Cour-Palais double-plate penetration equation was compared to the modified Cour-Palais single-plate penetration equation. Then the predictions from each of the seven double-plate penetration equations were compared to each other for a chosen shield design. Finally, these results from the equations were compared with test results performed at the NASA Marshall Space Flight Center. Because the different equations predict a wide range of projectile diameters at any given velocity, it is very difficult to choose the "right" prediction equation for shield configurations other than those exactly used in the equations' development. Although developed for various materials, the penetration equations alone cannot be relied upon to accurately predict the effectiveness of a shield without using hypervelocity impact tests to verify the design.

14. SUBJECT TERMS	15. NUMBER OF PAGES
Whipple shield penetration equations, double-plate penetration equations, Cour-Palais equation, Nysmith equation, Lundeberg-Stern-Bristow equation, Burch equation, Wilkinson equation, meteoroids, orbital debris, hypervelocity impact	36
	16. PRICE CODE A03

17. SECURITY CLASSIFICATION OF REPORT	18. SECURITY CLASSIFICATION OF THIS PAGE	19. SECURITY CLASSIFICATION OF ABSTRACT	20. LIMITATION OF ABSTRACT
Unclassified	Unclassified	Unclassified	Unlimited

National Aeronautics and
Space Administration
AD33
George C. Marshall Space Flight Center
Marshall Space Flight Center, Alabama
35812